# Study on distribution of long-period stacking ordered phase in Mg–Gd–Y–Zn–Zr alloy using friction stir processing

Q. Yang [a], B.L. Xiao [a,*], D. Wang [a], M.Y. Zheng [b], Z.Y. Ma [a,**]

[a] Shenyang National Laboratory for Materials Science, Institute of Metal Research, Chinese Academy of Sciences, Shenyang 110016, China
[b] School of Materials Science and Engineering, Harbin Institute of Technology, Harbin 150001, China

## ARTICLE INFO

## ABSTRACT

Friction stir processing (FSP) was applied to Mg–Gd–Y–Zn–Zr casting at various process parameters to study the influence of heat and deformation conditions on the distribution of long-period stacking ordered (LPSO) phase. FSP resulted in grain refinement, fundamental elimination of $\beta$-$Mg_3RE$ eutectics and formation of LPSO phase. Various distributions of LPSO phase, including no LPSO phase, LPSO phase both at the grain boundaries and within the grains and LPSO phase only within the grains could be obtained after FSP at the investigated process parameters. Based on the microstructure analyses and formation mechanism of LPSO phase, this varied distribution is believed to be caused by the combined influence of temperature, plastic strain and cooling rate. Detailed influence of these factors on the distribution of LPSO phase was discussed.

© 2014 Elsevier B.V. All rights reserved.

## 1. Introduction

Mg–Gd–Zn based alloys have received considerable attention in recent years [1–5], because of their superior mechanical properties provided by the special microstructure, especially the long-period stacking ordered (LPSO) phase. Recent studies revealed that the distribution of LPSO phase influenced mechanical properties greatly [6,7]. While the grain boundary distributed LPSO phase could improve ductility, the LPSO lamellae within the grains could enhance yield strength. This indicates that, besides the grain size, texture, and the size of LPSO phase, the distribution of LPSO phase may play an important role in the mechanical property optimization of Mg–Gd–Zn based alloys.

In Mg–Gd–Zn based alloys, the LPSO phase forms mainly in two ways: (1) transformation from $\beta$ phase and (2) precipitation from the supersaturated matrix. The transformation occurs at above 425 °C [8], with the transformed LPSO phase being mainly distributed at the grain boundaries. The precipitation occurs at above 350 °C, with the LPSO lamellae developing on the bases of stacking faults (SFs), and growing and coarsening with increasing annealing time and temperature [1,9,10]. The precipitated LPSO phase can be distributed both at the grain boundaries and within the grains [11].

During solution treatment of Mg–Gd–Zn based cast alloys, the solute segregation in grain boundary particles favors the transformation [12]. As a result, the LPSO phase is distributed mainly at the grain boundaries [1]. Small amounts of LPSO phase can extend into the grains by prolonging the annealing time or decreasing cooling rate [4,6,13]. During subsequent plastic deformation, the already formed LPSO phase can only be refined, thus its grain boundary distribution is seldom modified [14,15]. In our recent study, as a result of high temperature severe plastic deformation, friction stir processing (FSP) can eliminate solute segregation in Mg–Gd–Y–Zn–Zr casting and enhance precipitation of LPSO phase, leading to the distribution of LPSO phase only within the grains [16].

From the above statements, it is clear that the distribution of LPSO phase is closely related to temperature, plastic deformation and cooling rate. Therefore, investigating the relationship between these factors and the formation of LPSO phase is essential to control the distribution of LPSO phase and further enhance the mechanical properties of the Mg–Gd–Zn based alloys.

FSP is a short-route technique for microstructural modification [17–20]. The high temperature severe plastic deformation generated by FSP can dissolve the eutectics, refine particles, and alleviate severe solute segregation in cast magnesium alloys. Besides, the temperature, deformation and cooling rate during FSP can be varied by controlling the process parameter, e.g. the rotation rate and traverse speed. Moreover, the heat and deformation conditions also vary in local regions of the stir zone (SZ) [21–24]. Consequently, various microstructures can be obtained in the SZ by FSP [25–28]. It is therefore expected that FSP is an ideal method to study the relationship between the processing conditions (temperature, deformation and cooling rate) and the distribution of LPSO phase.

* Corresponding author. Tel.: +86 24 83978630; fax: +86 24 23971749.
** Corresponding author. Tel./fax: +86 24 83978908.
E-mail addresses: blxiao@imr.ac.cn (B.L. Xiao), zyma@imr.ac.cn (Z.Y. Ma).

In this study, FSP was applied to a cast Mg–Gd–Y–Zn–Zr alloy and the microstructure at different process parameters were systematically investigated. The aim is to elucidate the relationship between heat and deformation conditions and the formation of LPSO phase and establish the processing methods for controlling the distribution of LPSO phase.

## 2. Experimental

6 mm thick Mg–9.4Gd–4.1Y–1.2Zn–0.4Zr (wt%) cast plates were subjected to FSP. A conventional tool with a shoulder 20 mm in diameter, a threaded conical pin 8 mm in root diameter and 4.3 mm in length was used. FSP was carried out at various rotation rates and traverse speeds, as summarized in Table 1. Temperature histories were measured below the SZ using K-type thermocouples, which were embedded 4.3 mm below the plate surface in the centerline of the SZ.

Specimens for microscopy were machined from the cross-section of the SZ perpendicular to the FSP direction. Microstructural characterization was conducted by optical and transmission electron microscopy (OM and TEM, FEI Tecnai G$^2$ 20) in the centerline of the SZ at 0.2, 2.2 and 4.2 mm below the plate surface, i.e. the top, center and bottom regions, respectively. Specimens for OM were prepared by mechanical polishing and etching using a solution of 4.2 g picric acid+10 mL acetic acid+70 mL ethanol+10 mL water. Thin foils for TEM were prepared by low-energy ion milling. The volume fractions of second-phase particles were analyzed by an image analysis software (Image-Pro Plus 6.0).

## 3. Results

### 3.1. Microstructure

As shown in Fig. 1a, microstructure of the as-cast Mg–Gd–Y–Zn–Zr alloy is characterized by coarse α-Mg grains and large grain boundary irregular β-Mg$_3$RE eutectics in a dark contrast and a small number of LPSO particles in a gray contrast, as reported previously [16]. In addition, the fine lamellae observed within the

grains were determined to be the SFs by selected area electron diffraction (SAED), as shown in Fig. 1b.

Fig. 2 shows macrographs of the FSP samples. A basin-shaped SZ with a wide top region was observed at all process parameters. According to the contrast difference and the contributions of the shoulder and pin in formation of the SZ, all the SZs can be divided into two sub-zones: the shoulder-driven zone (SDZ) in the upper region and the pin-driven zone (PDZ) in the lower region [29–31]. As shown in Fig. 2a and b, the SDZ in a dark contrast was evidently observed and occupied half the SZ in FSP 1500-25 and 2000-25 samples. Higher magnification images of the two samples revealed voids at the SDZ/PDZ interface, as indicated by arrows in Fig. 2g and h, suggesting insufficient material flow between the SDZ and PDZ [30]. As the rotation rate increased, voids were eliminated, the SDZ expanded to almost the whole SZ, and the PDZ significantly shrank into the narrow bottom region, as shown in Fig. 2c and d. In the FSP 3000-25 sample, a light etching region was even observed to extend from the bottom to the upper region of the SZ (as marked by the dashed line in Fig. 2d), indicating the occurrence of upward material flow. This is coincident with previous study, which showed that vertical material flow can be generated when using a threaded conical pin at a high rotation rate [32,33]. At a constant rotation rate of 2500 rpm, the PDZ expanded as the traverse speed increased (Fig. 2c, e and f).

Fig. 3 shows the variation of grain size in different regions of the SZ with the process parameter. Significant grain refinement occurred after FSP. Gradient grain size was observed in all the SZs with the largest grains and grain size deviation in the top region and the finest in the bottom region. In the FSP 1500/25 sample, the grains were the finest with a size of 2.8 μm in the bottom region. The grain size in the top and center regions increased with increasing the rotation rate and decreasing the traverse speed, which is coincident with the change of heat input with the process parameter. However, grain size in the bottom region changed slightly with the process parameter.

Fig. 4 shows OM images of the top region in the SZ at various parameters. Nearly equiaxed grains with fine lamellae in the grains were observed. The grain sizes in the top regions for the FSP 1500-25, FSP 2000-25, FSP 2500-25, FSP 3000-25, FSP 2500-50 and FSP 2500-100 samples are 11.7 ± 2.4 μm, 22.1 ± 3.8 μm, 27.0 ± 2.4 μm,

**Table 1**
FSP parameters and sample definition for Mg–Gd–Y–Zn–Zr casting.

| Sample definition | 1500-25 | 2000-25 | 2500-25 | 3000-25 | 2500-50 | 2500-100 |
|---|---|---|---|---|---|---|
| Rotation rate (rpm) | 1500 | 2000 | 2500 | 3000 | 2500 | 2500 |
| Traverse speed (mm/min) | 25 | 25 | 25 | 25 | 50 | 100 |
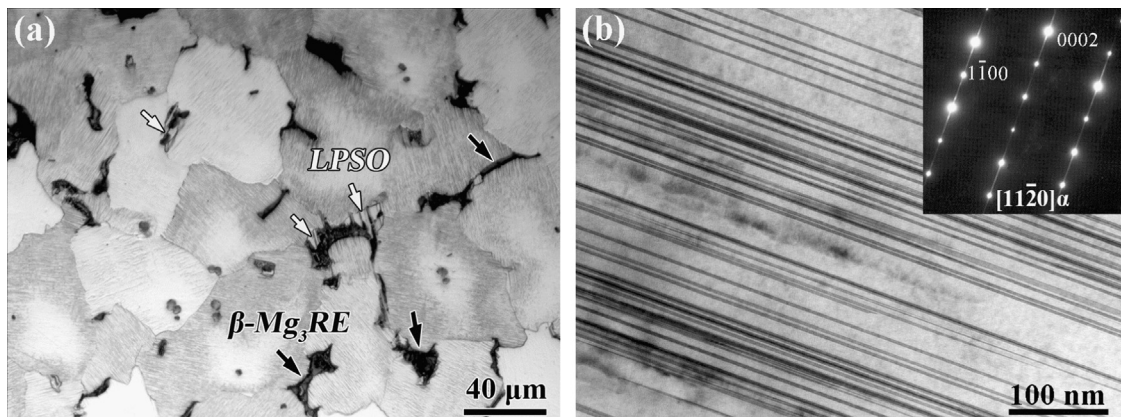


**Fig. 1.** (a) OM and (b) TEM images of as-cast Mg–Gd–Y–Zn–Zr alloy.
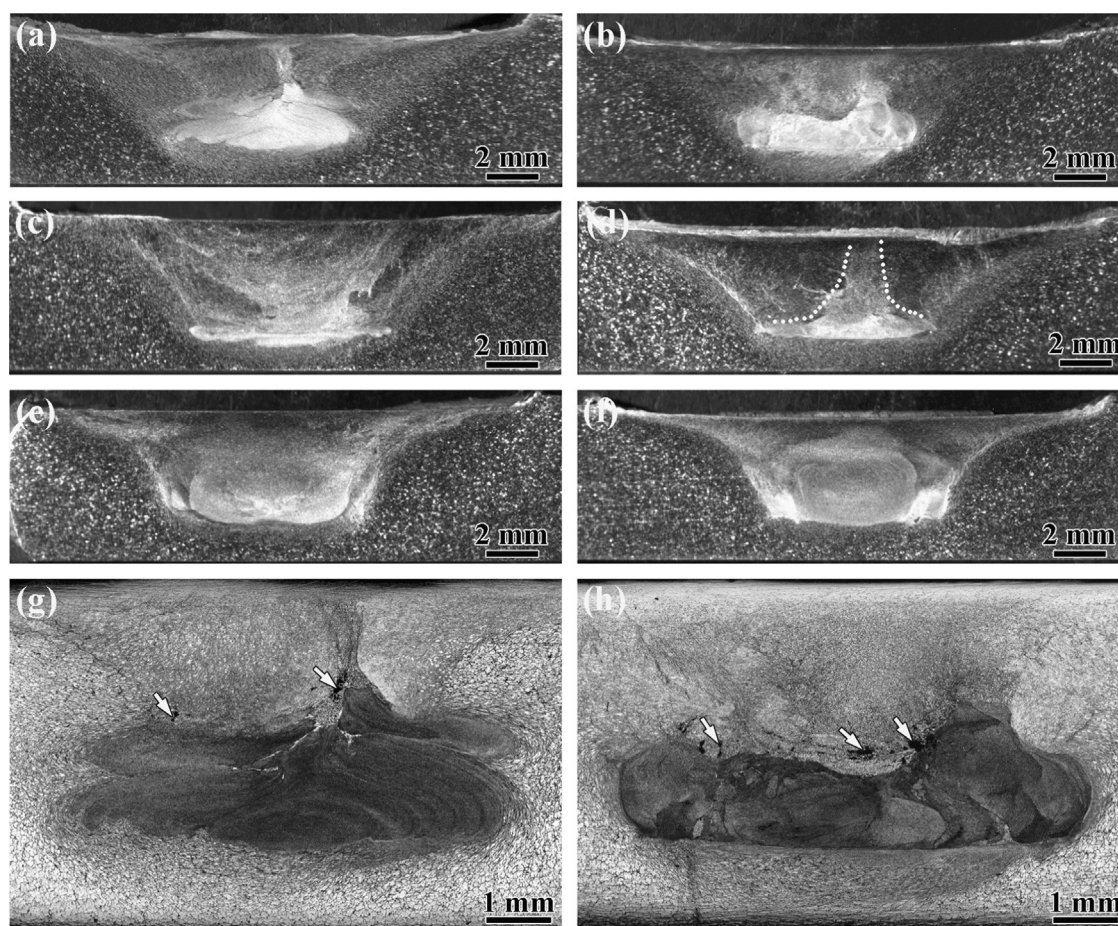
**Fig. 2.** Optical macrographs of the SZs at various parameters: (a) 1500-25, (b) 2000-25, (c) 2500-25, (d) 3000-25, (e) 2500-50, and (f) 2500-100; (g) a magnified image of (a), (h) a magnified image of (b) (the advancing side is on the right).

30.0 ± 7.1 μm, 20.8 ± 5.2 μm, 17.8 ± 3.1 μm, respectively. Except for the FSP 1500-25 sample with the gray LPSO particles ~5 μm in size in the lower part of Fig. 4a, generally no grain boundary particles were observed. Typical TEM images of the fine lamellae within the grains in this region are shown in Fig. 5. According to the SAED patterns in Fig. 5a and HRTEM image in Fig. 5b, the fine lamellae were identified to be SFs.

OM images of the center region in the SZ at various parameters are shown in Fig. 6. The grain sizes in the center regions for the FSP 1500-25, FSP 2000-25, FSP 2500-25, FSP 3000-25, FSP 2500-50 and FSP 2500-100 samples are 9.0 ± 2 μm, 13.4 ± 3.3 μm, 17.0 ± 3.5 μm, 20.3 ± 5.0 μm, 15.7 ± 2.6 μm, 15.5 ± 2.6 μm, respectively. Grain boundary distributed particles with both gray and/or dark contrasts were observed at all the investigated process parameters with their volume fraction listed in Table 2. Combining the subsequent TEM images with SAED patterns, the phase with a dark contrast in OM images is identified as the β phase, while the phase with a gray contrast is the LPSO phase. In the FSP 1500-25 sample, fine LPSO and β particles were heterogeneously distributed, besides, fine lamellae were observed only within the grains near the particles (Fig. 6a). As the rotation rate increased, the grain boundary particles and grains with fine lamellae tended to distribute uniformly. In the FSP 2000-25 sample, only LPSO particles with a high volume fraction of 8.9% and a large size of ~10 μm in length were distributed uniformly (Fig. 6b). At a higher rotation rate of 2500 rpm, the LPSO particles tended to be distributed in streamlines (Fig. 6c). However, in the FSP 3000-25 sample, coarse β particles always associated with LPSO particles with a total volume fraction of 9.9% appeared and were uniformly distributed, as shown in Fig. 6d. At a constant rotation rate of 2500 rpm, the LPSO particles tended to be distributed uniformly as

the traverse speed increased from 25 to 100 mm/min (Fig. 6c, e and f), while β particles appeared at 100 mm/min (Fig. 6f). Besides, the volume fraction of grain boundary particles increased slightly as the traverse speed increased (Table 2).

Fig. 7 shows TEM images of the center region in the SZ at various process parameters. In FSP 1500-25 sample, the LPSO particles were identified to be mainly of the 18R structure by SAED patterns (Fig. 7a), as were the LPSO phases at other process parameters. In addition, the irregularly-shaped β particles were determined to be Mg$_3$RE phase by SAED patterns in Fig. 7a, the same to that in the as-cast alloy. This indicates that the β particles observed in FSP samples were the remnant particles. The fine lamellae within the grains were determined to be LPSO phase at all the investigated parameters, but the average width of LPSO lamellae was almost unchanged with the process parameter, which was ~20 nm (Fig. 7b–d).

As shown in Fig. 8, uniform and fine microstructure was observed at all the investigated parameters in the bottom region of the SZ. The grain sizes in the bottom regions for the FSP 1500-25, FSP 2000-25, FSP 2500-25, FSP 3000-25, FSP 2500-50 and FSP 2500-100 samples are 2.8 ± 0.3 μm, 4.0 ± 0.6 μm, 6.2 ± 0.9 μm, 6.2 ± 1.4 μm, 6.2 ± 1.3 μm, 6.3 ± 1.1 μm, respectively. At a constant traverse speed of 25 mm/min, fine and dispersed grain boundary particles were observed at all rotation rates and their size and volume fraction increased with increasing the rotation rate from 1500 to 3000 rpm (Fig. 8a–d and Table 3). The particles at the lowest rotation rate of 1500 rpm can hardly be distinguished, while those at higher rotation rates with a gray contrast were determined to be only LPSO phase by additional TEM identification (not shown). At a constant rotation rate of 2500 rpm, the volume fraction of LPSO particles decreased substantially with increasing the traverse speed
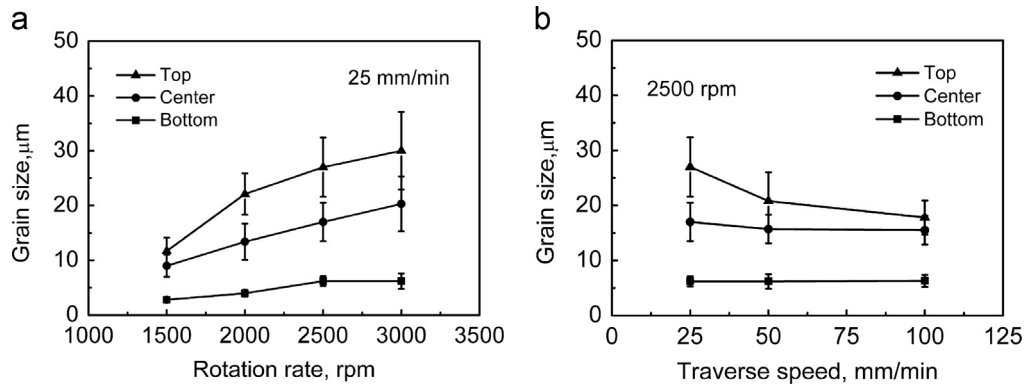
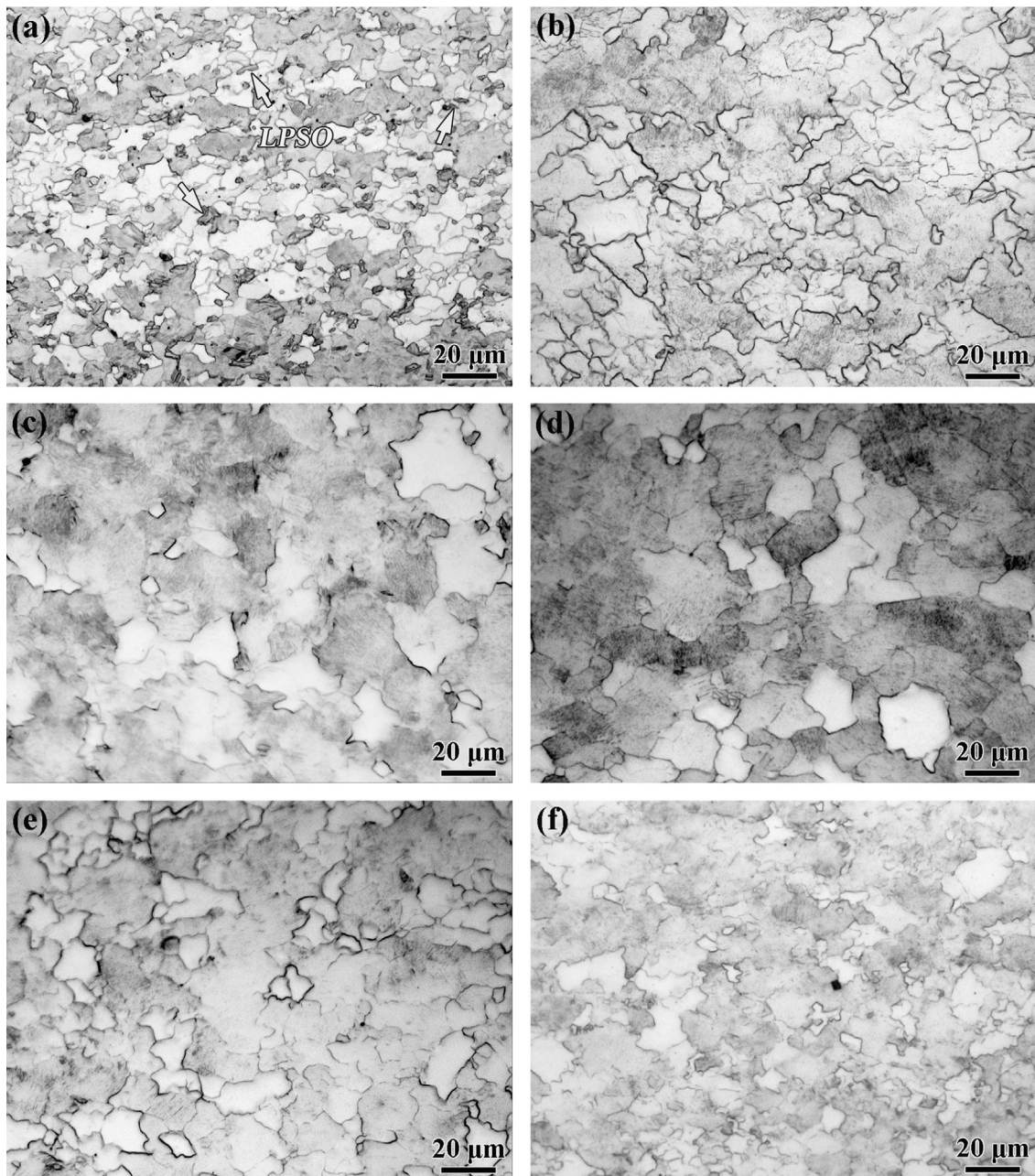**Fig. 3.** Variation of grain size with (a) rotation rate and (b) traverse speed at different regions of the SZ.



**Fig. 4.** OM images of the top region in the SZ at: (a) 1500–25, (b) 2000–25, (c) 2500–25, (d) 3000–25, (e) 2500–50, and (f) 2500–100.
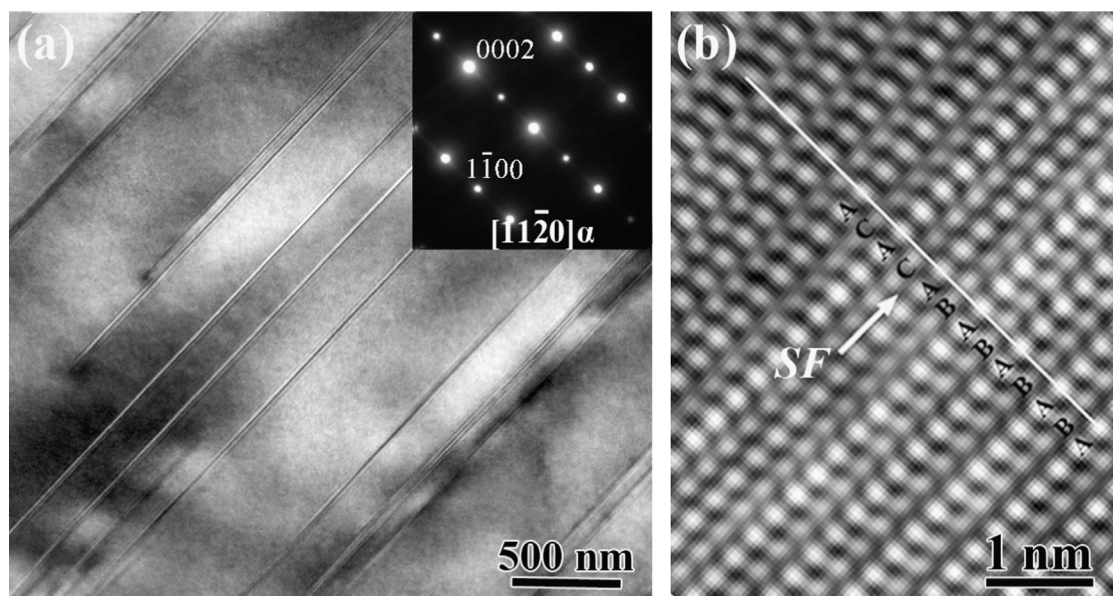
**Fig. 5.** (a) TEM and (b) HRTEM images of the lamellae with the electron beam parallel to $\langle 11-20 \rangle_\alpha$ of the top region in the SZ of FSP 3000-25 sample.

from 25 to 100 mm/min, and LPSO particles could even not be observed at 100 mm/min, as shown in Fig. 8c, e and f and Table 3.

Fig. 9 shows TEM images of the bottom region in the SZ at various parameters. The fine grain boundary particles in the FSP 1500-25 sample (indicated by arrows in Fig. 9a) were identified to be only the LPSO phase by SAED patterns. LPSO lamellae were formed within the grains at all process parameters. The average width of LPSO lamellae varied with the process parameter: the width of LPSO lamellae increased from ∼30 to 300 nm as the rotation rate increased from 1500 to 3000 rpm at a constant traverse speed of 25 mm/min (Fig. 9a–c), and it decreased from ∼200 nm at 25 mm/min to ∼50 nm at 100 mm/min at a constant rotation rate of 2500 rpm (Fig. 9b and d). Besides, the absence of LPSO particles at the grain boundaries in the FSP 2500-100 sample in Fig. 8f was further confirmed.

### 3.2. Temperature history

Fig. 10 shows the temperature histories recorded below the SZ at various parameters. The peak temperature reached above 370 °C at all process parameters, which is higher than the formation temperature of LPSO phase (∼350 °C). The peak temperature and high-temperature duration increased with the rotation rate and decreased with the traverse speed. At a constant traverse speed of 25 mm/min, the peak temperature increased from 370 °C at 1500 rpm to 460 °C at 3000 rpm, and the duration above 300 °C increased from ∼44 s at 1500 rpm to ∼64 s at 3000 rpm. At a constant rotation rate of 2500 rpm, the peak temperature decreased from 450 °C at 25 mm/min to 426 °C at 100 mm/min, and the duration above 300 °C decreased markedly from ∼58 s at 25 mm/min to ∼17 s at 100 mm/min. Besides, increasing the traverse speed can significantly increase the cooling rate. The cooling rate was ∼3 K/s at 25 mm/min, while it was ∼8.6 K/s at 100 mm/min.

## 4. Discussion

As a result of high temperature severe plastic deformation that induces dynamic recrystallization, particle breakup, accelerated diffusion and decreased diffusion distance of solutes, generally fine-grained microstructure with predominant LPSO phase was obtained in FSP Mg–Gd–Y–Zn–Zr casting at all the investigated process parameters. This is similar to our previous studies [16,34].

Moreover, various distributions of LPSO phase, i.e., no LPSO phase, LPSO phase both at the grain boundaries and within the grains, and LPSO phase only within the grains can be achieved after FSP, suggesting that FSP is an effective method to control the distribution of LPSO phase. The inhomogeneous microstructure with varied grain size and distribution of LPSO phase in all the SZs reflected the local variation of heat and deformation conditions in the SZ.

The gradient grain size in all the SZs (Fig. 3) suggested the existence of a temperature gradient, with the temperature being the highest at the surface and decreasing with increasing the distance from the SZ surface. This is confirmed by both experimental and simulation studies [25,27,35–37]. In addition, simulation on the equivalent plastic strain distribution in the SZ revealed that the highest strain was located in the PDZ, whereas the plastic strain was lower in the SDZ and decreased with increasing the distance from the SZ surface [21]. Guerdoux et al. [23] also suggested that high equivalent strain was concentrated in the bottom of the SZ with a threaded pin.

It is seen from Fig. 2 that, in all FSP samples, the top and center regions are located in the SDZ, and the bottom region is located in the PDZ. Therefore, the heat and deformation conditions in different regions of the SZ during FSP can be speculated as: (1) the top region underwent the highest temperature and a medium strain; (2) the center region experienced a medium temperature and the lowest strain and (3) the bottom region experienced the lowest temperature but the highest strain. As for the influence of the FSP parameters, increasing the rotation rate generally resulted in the increase of temperature and strain, increasing the traverse speed resulted in decreased temperature and strain, and increased cooling rate [17,25–27,36,38–42].

Based on the above analyses, the varied distribution of LPSO phase in the SZ should be caused by the variation of heat and deformation conditions. In the following section, the formation of LPSO phase in different regions of the SZ is first analyzed, then the influence of heat and deformation conditions on the distribution of LPSO phase is clarified.

### 4.1. Relationship between formation of LPSO phase and FSP parameter

In the top region of the SZ, due to the highest temperature rise and large plastic strain, breakup and complete dissolution of LPSO
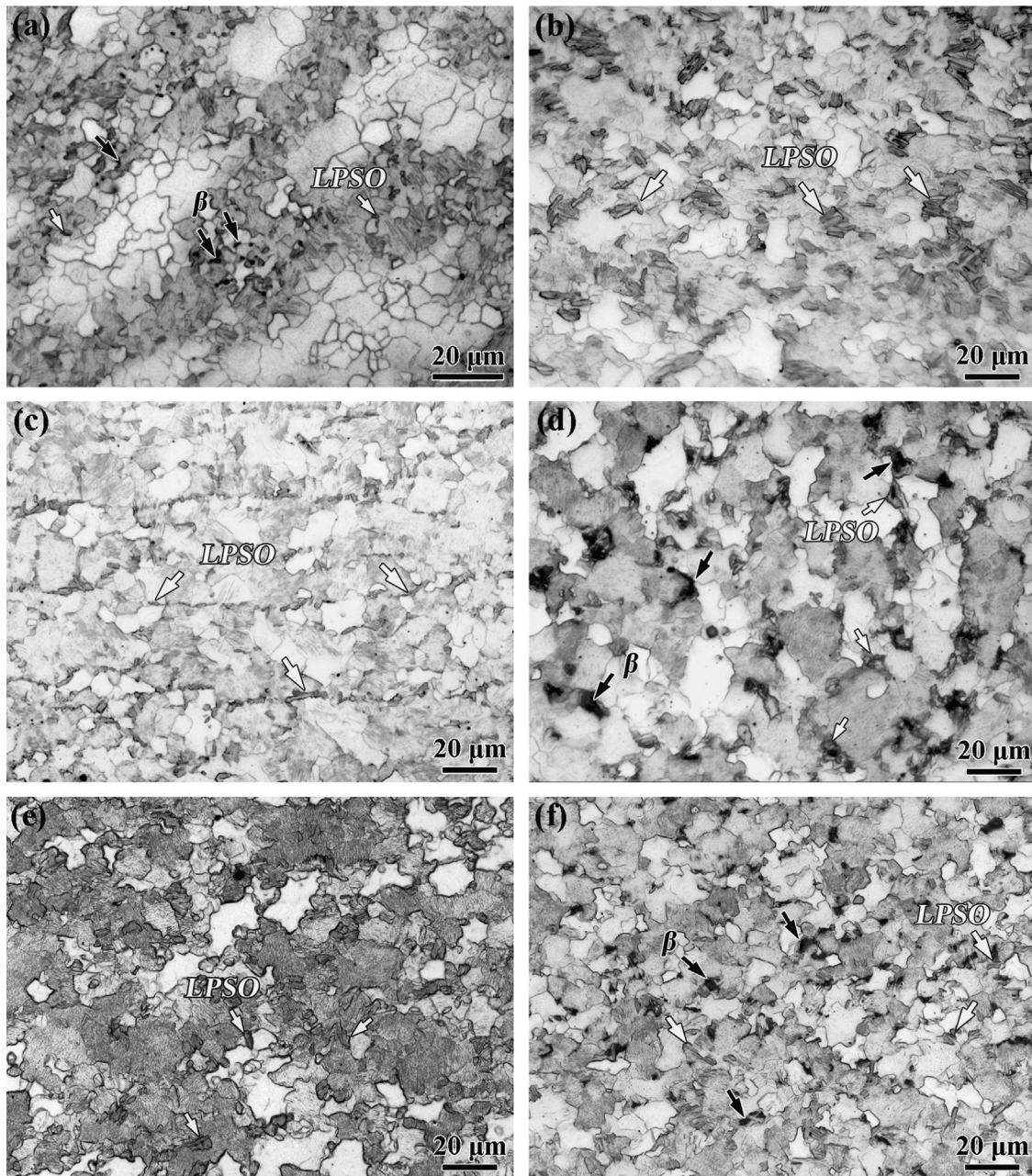
**Fig. 6.** OM images of the center region in the SZ at: (a) 1500-25, (b) 2000-25, (c) 2500-25, (d) 3000-25, (e) 2500-50, and (f) 2500-100.

**Table 2**
Volume fraction of grain boundary particles in the center regions of FSP samples.

| FSP sample | 1500-25 | 2000-25 | 2500-25 | 3000-25 | 2500-50 | 2500-100 |
|---|---|---|---|---|---|---|
| Volume fraction, % | 2.6 | 8.9 | 5.0 | 9.9 | 5.9 | 6.3 |

and β particles occurred, resulting in α-Mg single phase structure at all processing parameters, as shown in Fig. 4. It should be mentioned that, only SFs formed in the top region, while LPSO lamellae formed in the center and bottom regions (Figs. 7 and 9). Formation of only SFs in the top region indicated the short high-temperature duration in the top region that restricts further development of LPSO phase. This is consistent with previous

report that the top region of the SZ experienced the fastest cooling rate during FSP [27]. As the heat input decreased, the region with α-Mg single phase microstructure narrowed. This is evidenced by the narrow top region with no particles in FSP 1500-25 sample (Fig. 4a).

In the center region of all the SZs, the grain boundary distributed LPSO particles and fine LPSO lamellae with the width almost unchanged with the process parameter suggested that, due to both lower peak temperature and plastic strain than the top region, phase dissolution cannot occur effectively in this region. The particles then experienced mainly breakup and transformation from β into LPSO phase, while only a small amount of β particles were dissolved in the center region. As a result, fine LPSO lamellae were formed at all process parameters. The observed irregularly-shaped β particles always associated with LPSO particles further confirmed the occurrence of transformation mechanism, and also indicated the incomplete transformation process.
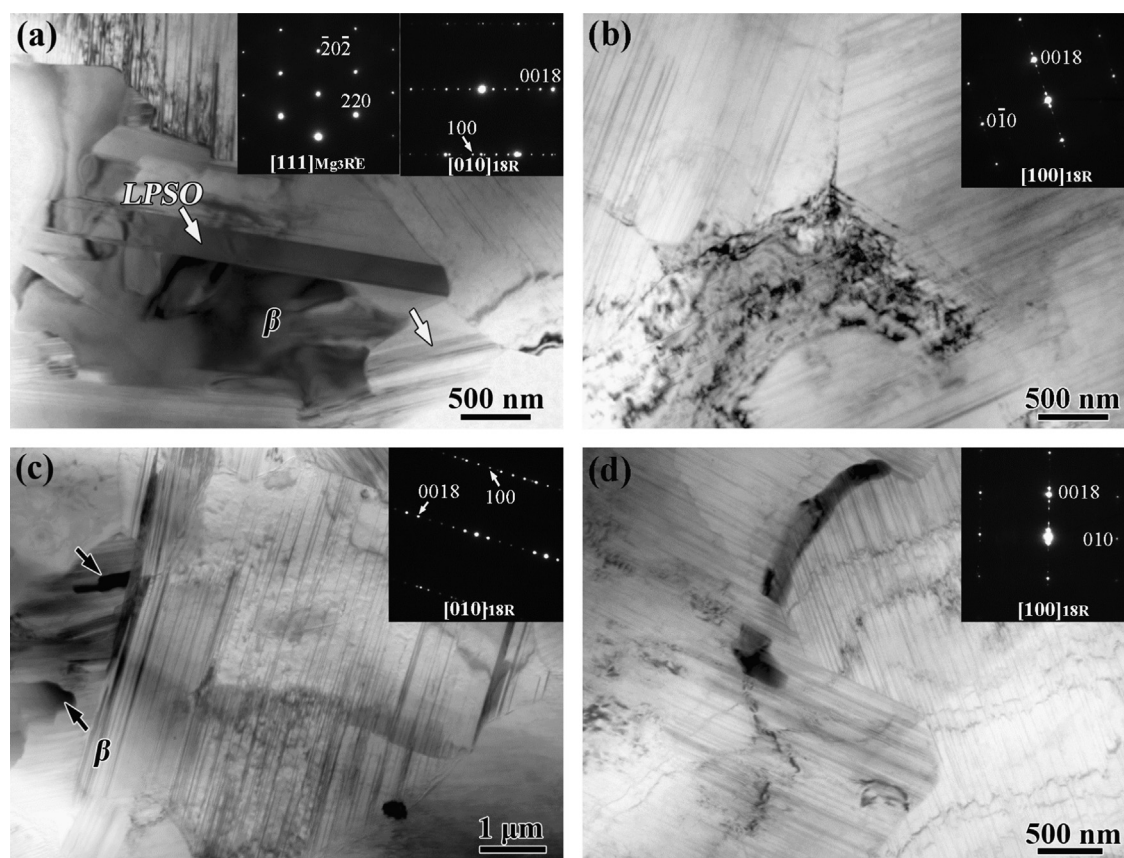
**Fig. 7.** TEM images of the center region in the SZ at: (a) 1500-25, (b) 2500-25, (c) 3000-25 and (d) 2500-100.

It should be mentioned that, although the temperature experienced in the center region is not the lowest in the SZ, remnant β particles are only observed in this region. The lowest plastic strain experienced in the center region should be the main reason for remnant β particles. The low plastic strain cannot exert effective breakup of β particles, thus it will take longer time for the coarse broken β particles in the center region to achieve complete transformation or dissolution. Moreover, the LPSO lamellae in the center region with low plastic strain are finer than that in the bottom region for all the SZs (Figs. 7 and 9). These suggest that, large plastic strain is much more effective than high temperature in achieving both phase transformation and dissolution.

At the lowest rotation rate of 1500 rpm, the insufficient material flow in the center region caused locally low plastic strain and probably low temperature, resulting in incomplete transformation process. This is evidenced by the heterogeneously distributed remnant β particles (Fig. 6a). Besides, particle dissolution also occurred locally, resulting in distribution of LPSO lamellae only within the grains near the particles. As the rotation rate increased, the temperature and plastic deformation increased, thus enhancing the transformation process and homogeneous distribution of LPSO lamellae (Fig. 6b–f and Fig. 7). The transformation process completed at a rotation rate of 2000 rpm (Fig. 6b). As the rotation rate increased to 2500 rpm, the increased plastic strain would enhance particle dissolution and induce additional deformation of the transformed LPSO particles. As a result, similar to that observed in extruded or rolled Mg–Gd–Zn based alloys [14,15], LPSO particles were distributed in streamlines with a lower volume fraction than that in FSP 2000-25 sample (Fig. 6c and Table 2). However, further increasing the rotation rate to 3000 rpm caused considerable upward material flow (Fig. 2d). The change of material flow may alter the local deformation condition. The high volume fraction particles with remnant β particles in the center

region of FSP 3000-25 sample indicated the locally low plastic strain, which results in incomplete transformation.

At the constant rotation rate of 2500 rpm, increasing the traverse speed resulted in decreased peak temperature and strain, and increased cooling rate. As seen from Fig. 10, the local peak temperature did not change much with the traverse speed, but the cooling rate increased largely with the traverse speed. Thus, the remnant β particles in the center region of the FSP 2500-100 sample (Fig. 6f) should result mainly from the increased cooling rate that restricts the transformation. Moreover, the decreased plastic strain restricts both particle dissolution and additional deformation of particles, resulting in uniformly distributed particles with increased volume fraction at increased traverse speed (Fig. 6c, e, f and Table 2).

The bottom region of the SZ experienced the lowest temperature but high plastic strain during FSP, thus the finest microstructure was obtained in this region. Different from that in the center region where the process parameter cannot change the distribution of LPSO phase, the distribution of LPSO phase in the bottom region can be substantially affected by the process parameter. For example, in the FSP 2500-100 sample, the LPSO phase was distributed only within the grains, while the grain boundary distributed LPSO particles were observed in other samples (Fig. 8).

The distribution difference of LPSO phase in the bottom region with the process parameter should not result from the differed local temperature or plastic strain. The local peak temperature experienced in FSP 2500-100 sample is intermediate in all samples (Fig. 10), and the plastic strain in FSP 2500-100 sample should also not be the lowest because of the intermediate rotation rate. The distinct difference between these samples is the shortest high-temperature duration and the largest cooling rate experienced in FSP 2500-100 sample (Fig. 10). This should be the main reason for the different distributions of LPSO phase. The distribution of LPSO
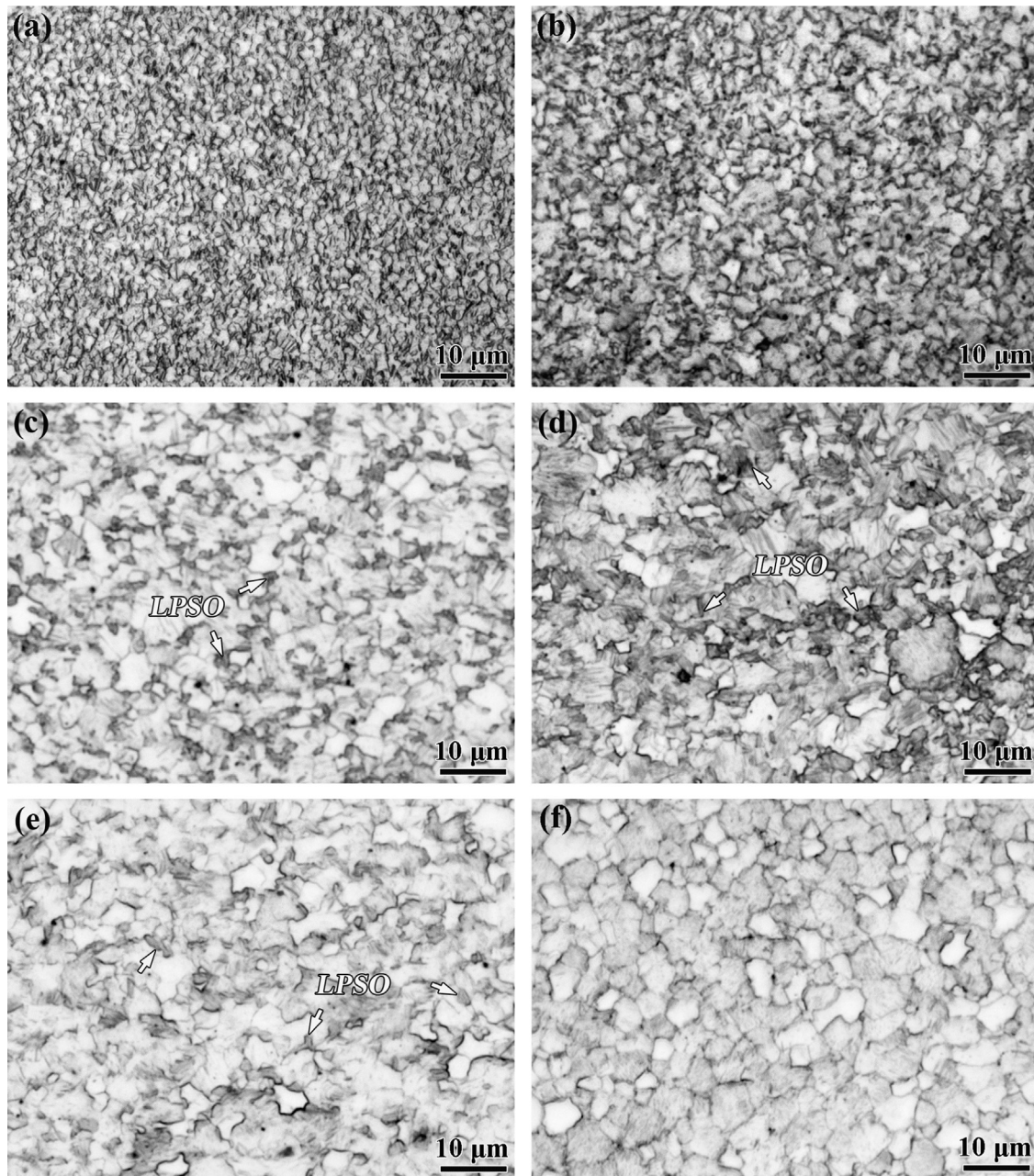
**Fig. 8.** OM images of the bottom region in the SZ at: (a) 1500-25, (b) 2000-25, (c) 2500-25, (d) 3000-25, (e) 2500-50, and (f) 2500-100.

**Table 3**
Volume fraction of grain boundary particles in the bottom region of FSP samples.

| FSP sample | 1500-25 | 2000-25 | 2500-25 | 3000-25 | 2500-50 | 2500-100 |
|---|---|---|---|---|---|---|
| Volume fraction, % | 1.2 | 4.0 | 4.2 | 7.2 | 1.3 | 0 |

phase only within the grains in FSP 2500-100 sample suggests that, all the particles could be dissolved in FSP 2500-100 sample with the shortest high-temperature duration. Accordingly, the observed LPSO phase in the bottom region should form only through precipitation, rather than transformation for all FSP samples. The cooling rate should then be the main factor influencing the distribution of LPSO phase in the bottom region. The LPSO phase precipitated only within the grains at high cooling rate,

while both at the grain boundaries and within the grains at lower cooling rate. Therefore, the traverse speed that significantly influences the cooling rate can control the distribution of LPSO phase in the bottom region of the SZ.

The distribution variation of LPSO phase with the cooling rate in the bottom region should stem from two aspects. First, the interface between LPSO phase and the matrix is coherent [1,43], such coherency favored homogeneous precipitation of LPSO phase. Second, the undercooling can influence the driving force for precipitation, with the driving force increasing with increasing the undercooling [44]. For the FSP 2500-100 sample with a high cooling rate, the large undercooling renders high driving force for LPSO precipitation, therefore homogeneous precipitation of LPSO phase occurs. For other FSP samples with lower cooling rates, the low undercooling causes insufficient driving force for LPSO precipitation. Thus, the nucleation of LPSO phase at the grain boundaries that can reduce the nucleation barrier was promoted.
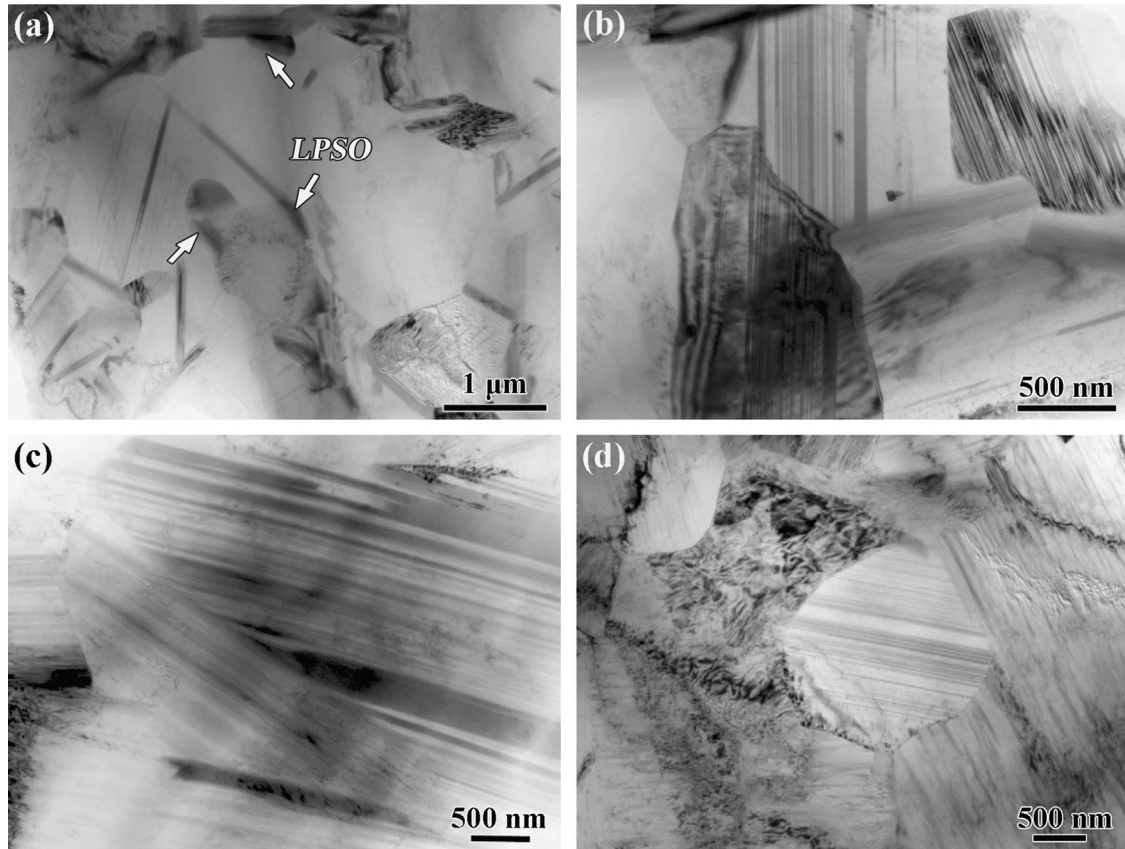
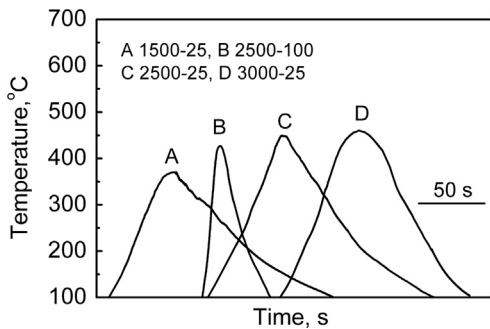**Fig. 9.** TEM images of the bottom region in the SZ at: (a) 1500-25, (b) 2500-25, (c) 3000-25, and (d) 2500-100.



**Fig. 10.** Temperature histories of the FSP Mg–Gd–Y–Zn–Zr casting at various parameters.



**Fig. 11.** Schematic diagrams showing the influence of temperature, plastic strain and cooling rate on the distribution of LPSO phase in FSP Mg–Gd–Y–Zn–Zr casting.

In addition, the coarsening of LPSO phase also occurred at decreased cooling rate and increased high-temperature duration. This is evidenced by the coarsening of LPSO particles and widening of LPSO lamellae at increased rotation rate and decreased traverse speed (Fig. 9).

The different phase evolution process occurred between the bottom and center region should be caused mainly by the different plastic strain. It has been proved that plastic deformation can enhance phase transformation or dissolution [20,45,46]. Recently, an effective temperature was proposed by Zhang et al. to show the contribution of severe deformation effect of FSP, which was much higher than the actual temperature experienced during FSP [47]. In this case, although the temperature is low in the bottom region, the large plastic strain could contribute high effective temperature that can enable complete phase dissolution. Besides, the large plastic strain can exert thorough breakup of particles and also accelerate solute diffusion, thus homogeneous solute distribution can be achieved. While for 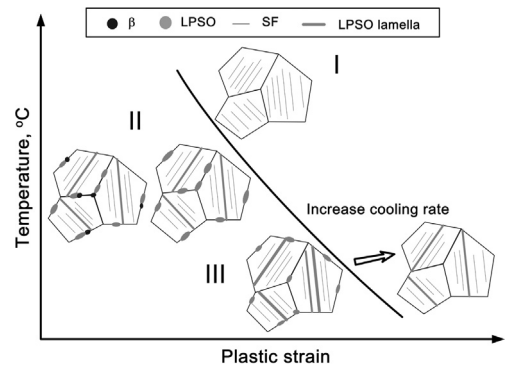the center region with low plastic strain, both the particle breakup extent and solute diffusion rate are lower than the bottom region, therefore, the short-range transformation from β to LPSO particles would prefer to occur.

### 4.2. Distribution control of LPSO phase

Based on the above discussions, distribution of LPSO phase is strongly controlled by its formation mechanism, which is influenced by the heat and deformation conditions. Fig. 11 illustrates a schematic influence of temperature, plastic strain and cooling rate on the distribution of LPSO phase. This also reflects the distribution of LPSO phase in the top, center and bottom regions of the SZ.

I. At high temperature, high plastic strain with high cooling rate, the phase dissolution occurs, resulting in α-Mg single phase microstructure.

II. At intermediate temperature and low plastic strain, the LPSO phase was formed mainly through transformation from β phase. Consequently, the LPSO phase was distributed mainly at the grain boundaries. The cooling rate had minor influence on the distribution of LPSO phase, but decreased plastic strain or increased cooling rate resulted in incomplete transformation process and thus remnant β particles after FSP.

III. At low temperature (above ~350 °C) and high plastic strain, complete particle dissolution occurs and the LPSO phase forms only by precipitation. The cooling rate exerts an important influence on the distribution of LPSO phase. LPSO formed both at the grain boundaries and within the grains at low cooling rate, while it formed only within the grains at high cooling rate.

It can be seen from Fig. 11 that, the distribution of LPSO phase at the grain boundaries can be easily obtained by both transformation and precipitation mechanisms in wide temperature and deformation ranges. This explains well the commonly observed grain boundary distributed LPSO phase in the solution-treated and plastically deformed Mg–Gd–Zn based alloys [3–5,8,13,15,48–51]. However, complete distribution of LPSO phase within the grains can be obtained only by the precipitation mechanism, which requires high plastic strain and high cooling rate at above ~350 °C. This requirement can be hardly achieved by solution treatment and other plastic deformation methods. In contrast, it can be achieved by FSP.

The distribution of LPSO phase in the top and center regions located in the SDZ cannot be substantially changed by the process parameter. However, distribution of LPSO phase in the bottom region located in the PDZ can be changed substantially by the traverse speed. Low traverse speed results in the distribution of LPSO phase both at the grain boundaries and within the grains, while high traverse speed results in the distribution of LPSO phase only within the grains. Moreover, to improve microstructure homogeneity of the SZ, the rotation rate should be further decreased to both decrease the grain size deference and enlarge the region of PDZ, as seen from Figs. 2 and 3. Because the rotation rate of 1500 rpm resulted in void defects (Fig. 2g), the material flow of Mg–Gd–Y–Zn–Zr casting should be improved to obtain a defect free SZ at rotation rates below 1500 rpm. The material flow can be improved by applying second pass FSP or using a tool with lower thermal conductivity [52,53]. The above speculations have been well verified in our previous studies, that uniform microstructure with LPSO phase distributed only within the grains can be obtained at a low rotation rate of 800 rpm and a high traverse speed of 100 mm/min by two-pass FSP or improved FSP tool [16,34].

## 5. Conclusions

FSP was applied to Mg–Gd–Y–Zn–Zr casting at rotation rates of 1500–3000 rpm and traverse speeds of 25–100 mm/min to study the influence of heat and deformation conditions on the distribution of LPSO phase. The main conclusions are summarized as follows:

1. FSP resulted in significant grain refinement, fundamental elimination of β-Mg₃RE eutectics and formation of LPSO phase. Parameter dependent gradient distribution of LPSO phase was obtained in all the SZs.

2. In the top region of the SZ, α-Mg single phase microstructure was observed at all process parameters. In the center region of the SZ, the LPSO phase was mainly distributed at the grain boundaries. In the bottom region of the SZ, the LPSO phase was distributed both at the grain boundaries and within the grains

at traverse speeds of 25 and 50 mm/min, but only within the grains at a traverse speed of 100 mm/min.

3. The distribution of LPSO phase in FSP samples is influenced by the temperature, plastic strain and cooling rate. While the distribution of LPSO phase at the grain boundaries can be obtained in wide ranges of temperature, plastic strain and cooling rate, distribution of LPSO phase only within the grains requires high plastic strain and high cooling rate at above ~350 °C.

## References

[1] M. Yamasaki, M. Sasaki, M. Nishijima, K. Hiraga, Y. Kawamura, Acta Mater. 55 (2007) 6798–6805.
[2] C. Xu, M.Y. Zheng, S.W. Xu, K. Wu, E.D. Wang, S. Kamado, G.J. Wang, X.Y. Lv, Mater. Sci. Eng. A 547 (2012) 93–98.
[3] D.D. Yin, Q.D. Wang, C.J. Boehlert, V. Janik, Y. Gao, W.J. Ding, Mater. Sci. Eng. A 546 (2012) 239–247.
[4] L. Zheng, C. Liu, Y. Wan, P. Yang, X. Shu, J. Alloys Compd. 509 (2011) 8832–8839.
[5] S. Zhang, G.Y. Yuan, C. Lu, W.J. Ding, J. Alloys Compd. 509 (2011) 3515–3521.
[6] C. Xu, M.Y. Zheng, K. Wu, E.D. Wang, G.H. Fan, S.W. Xu, S. Kamado, X.D. Liu, G.J. Wang, X.Y. Lv, Mater. Sci. Eng. A 559 (2012) 364–370.
[7] J. Wang, P. Song, S. Huang, F. Pan, Mater. Sci. Eng. A 563 (2013) 36–45.
[8] W.J. Ding, Y.J. Wu, L.M. Peng, X.Q. Zeng, G.Y. Yuan, D.L. Lin, J. Mater. Res. 24 (2009) 1842–1854.
[9] A. Ono, E. Abe, T. Itoi, M. Hirohashi, M. Yamasaki, Y. Kawamura, Mater. Trans. 49 (2008) 990–994.
[10] M. Nishida, Y. Kawamura, T. Yamamuro, Mater. Sci. Eng. A 375–377 (2004) 1217–1223.
[11] T. Honma, T. Ohkubo, S. Kamado, K. Hono, Acta Mater. 55 (2007) 4137–4150.
[12] Y.J. Wu, X.Q. Zeng, D.L. Lin, L.M. Peng, W.J. Ding, J. Alloys Compd. 477 (2009) 193–197.
[13] C. Xu, S.W. Xu, M.Y. Zheng, K. Wu, E.D. Wang, S. Kamado, G.J. Wang, X.Y. Lv, J. Alloys Compd. 528 (2012) 40–44.
[14] K. Liu, L.L. Rokhlin, F.M. Elkin, D. Tang, J. Meng, Mater. Sci. Eng. A 527 (2010) 828–834.
[15] Y.J. Wu, L.M. Peng, X.Q. Zeng, D.L. Lin, W.J. Ding, Y.H. Peng, J. Mater. Res. 24 (2009) 3596–3602.
[16] Q. Yang, B.L. Xiao, D. Wang, M.Y. Zheng, K. Wu, Z.Y. Ma, J. Alloys Compd. 581 (2013) 585–589.
[17] R.S. Mishra, Z.Y. Ma, Mater. Sci. Eng. R 50 (2005) 1–78.
[18] M.L. Santella, T. Engstrom, D. Storjohann, T.-Y. Pan, Scr. Mater. 53 (2005) 201–206.
[19] Z.Y. Ma, S.R. Sharma, R.S. Mishra, Mater. Sci. Eng. A 433 (2006) 269–278.
[20] A.H. Feng, Z.Y. Ma, Scr. Mater. 56 (2007) 397–400.
[21] S. Xu, X. Deng, Acta Mater. 56 (2008) 1326–1341.
[22] P. Asadi, R.A. Mahdavinejad, S. Tutunchilar, Mater. Sci. Eng. A 528 (2011) 6469–6477.
[23] S. Guerdoux, L. Fourment, Model. Simul. Mater. Sci. Eng. 17 (2009) 075001.
[24] H.H. Cho, S.T. Hong, J.H. Roh, H.S. Choi, S.H. Kang, R.J. Steel, H.N. Han, Acta Mater. 61 (2013) 2649–2661.
[25] K.O. Ishi, T.R. McNelley, Metall. Mater. Trans. A 36A (2005) 1575–1585.
[26] D.R. Ni, P. Xue, D. Wang, B.L. Xiao, Z.Y. Ma, Mater. Sci. Eng. A 524 (2009) 119–128.
[27] K.A.A. Hassan, P.B. Prangnell, A.F. Norman, D.A. Price, S.W. Williams, Sci. Technol. Weld. Join. 8 (2003) 257–268.
[28] M.A. Sutton, B. Yang, A.P. Reynolds, R. Taylor, Mater. Sci. Eng. A 323 (2002) 160–166.
[29] K. Kumar, S.V. Kailas, Mater. Sci. Eng. A 485 (2008) 367–374.
[30] Z. Zhang, B.L. Xiao, D. Wang, Z.Y. Ma, Metall. Mater. Trans. A 42A (2011) 1717–1726.
[31] W.J. Arbegast, Scr. Mater. 58 (2008) 372–376.
[32] M. Guerra, C. Schmidt, J.C. McClure, L.E. Murr, A.C. Nunes, Mater. Charact. 49 (2003) 95–101.
[33] B.C. Liechty, B.W. Webb, J. Mater. Process. Technol. 184 (2007) 240–250.
[34] Q. Yang, B.L. Xiao, Q. Zhang, M.Y. Zheng, Z.Y. Ma, Scr. Mater. 69 (2013) 801–804.
[35] X.X. Zhang, B.L. Xiao, Z.Y. Ma, Metall. Mater. Trans. A 42A (2011) 3229–3239.
[36] M.J. Peel, A. Steuwer, P.J. Withers, T. Dickerson, Q. Shi, H. Shercliff, Metall. Mater. Trans. A 37A (2006) 2183–2193.
[37] D.C. Hofmann, K.S. Vecchio, Mater. Sci. Eng. A 465 (2007) 165–175.
[38] G. Buffa, J. Hua, R. Shivpuri, L. Fratini, Mater. Sci. Eng. A 419 (2006) 381–388.
[39] P. Ulysse, Mach. Tool. Manuf. 42 (2002) 1549–1557.
[40] C.I. Chang, C.J. Lee, J.C. Huang, Scr. Mater. 51 (2004) 509–514.

[41] G. Buffa, J. Hua, R. Shivpuri, L. Fratini, Mater. Sci. Eng. A 419 (2006) 389–396.
[42] Z. Zhang, H.W. Zhang, Mater. Des. 30 (2009) 900–907.
[43] Y.M. Zhu, M. Weyland, A.J. Morton, K. Oh-ishi, K. Hono, J.F. Nie, Scr. Mater. 60 (2009) 980–983.
[44] D.A. Porter, K.E. Easterling, Phase Transformations in Metals and Alloys, 2nd ed., Chapman & Hall, London, 1992.
[45] H. Luo, Mater. Sci. Eng. A 528 (2011) 8259–8262.
[46] M. Murayama, Z. Horita, K. Hono, Acta Mater. 49 (2001) 21–29.
[47] Q. Zhang, B.L. Xiao, Z.Y. Ma, Mater. Chem. Phys. 139 (2013) 596–602.
[48] Y. Gao, Q. Wang, J. Gu, Y. Zhao, Y. Tong, D. Yin, J. Alloys Compd. 477 (2009) 374–378.
[49] D.J. Li, X.Q. Zeng, J. Dong, C.Q. Zhai, W.J. Ding, J. Alloys Compd. 468 (2009) 164–169.
[50] K. Liu, J. Zhang, H. Lu, D. Tang, L.L. Rokhlin, F.M. Elkin, J. Meng, Mater. Des. 31 (2010) 210–219.
[51] K. Yamada, Y. Okubo, M. Shiono, H. Watanabe, S. Kamado, Y. Kojima, Mater. Trans. 47 (2006) 1066–1070.
[52] A.H. Feng, B.L. Xiao, Z.Y. Ma, R.S. Chen, Metall. Mater. Trans. A 40A (2009) 2447–2456.
[53] R. Rai, A. De, H.K.D.H. Bhadeshia, T. DebRoy, Sci. Technol. Weld. Join. 16 (2011) 325–342.